16-20 July 2017, Charleston, South Carolina

Mars Atmospheric Conversion to Methane and Water: An Engineering Model of the Sabatier Reactor with Characterization of Ru/Al₂O₃ for Long Duration Use on Mars

Anne J. Meier[1], Malay G. Shah[2], Paul E. Hintze, Ph.D.[3], Anthony C. Muscatello, Ph.D.[4]
NASA, Kennedy Space Center, Florida, 32899, USA

Elspeth Petersen[5]
Iowa State University, Iowa, 50011, USA

The Atmospheric Processing Module (APM) is a Mars In-Situ Resource Utilization (ISRU) technology designed to demonstrate conversion of the Martian atmosphere into methane for use as rocket propellant for an ascent vehicle. The Martian atmosphere mainly consists of 95% carbon dioxide (CO_2) and residual argon and nitrogen. APM utilized cryocoolers for CO_2 acquisition from a simulated Martian atmosphere and pressure. The captured CO_2 was sublimated and pressurized as a feedstock into the Sabatier reactor, which converted CO_2 and hydrogen to methane and water. The Sabatier reaction occurred over a packed bed reactor filled with Ru/Al₂O₃ catalyst pellets. During performance testing at high flow rates, failure of the Sabatier catalyst occurred, which was detected by unwanted byproducts at elevated reaction temperatures. A Sabatier catalyst failure study was initiated after this event. This led to an effort to develop a model that could determine acceptable flow rates and predict the temperature profile in order to avoid catalyst damage and identify system tolerances. Validation of a computational model with experimental results also aids in long duration system development for reactor scaling purposes. This paper discusses the experimental results of the APM Sabatier tests, as well as a small scale Sabatier reactor that was set up for further model validation. The thermal and kinetic modeling approaches are discussed, as well as results of the APM catalyst characterization which included x-ray powder diffraction and x-ray photoelectron spectroscopy.

Nomenclature

Ac	=	Reactor cross-sectional area, m²
Al₂O₃	=	Aluminum oxide
APM	=	Atmospheric processing module
B	=	Particle shape factor, dimensionless
Bi	=	Biot number, (= h D_h 2^{-1} $keff^{-1}$), dimensionless
Cp	=	Heat capacity of mixed gas stream, J mol^{-1} K^{-1}
D_h	=	Hydraulic diameter, ($=Z_2 - Z_1$), m
D_p	=	Equivalent spherical pellet diameter, m
E_a	=	Activation energy, J mol^{-1}
f	=	Darcy friction factor, (= (0.79ln(Re)-1.64)$^{-2}$), dimensionless
GC	=	Gas chromatography
h	=	Convective heat transfer coefficient, W m^{-2} K^{-1}

---

[1] Chemical Engineer, Applied Science Branch, Mail Stop UB-R3-A.
[2] Thermofluid Engineer, Engineering Analysis Branch, NE-XY.
[3] Chemist, Applied Science Branch, Mail Stop UB-R3-A.
[4] Chemist, Applied Science Branch, Mail Stop UB-R3-A.
[5] Ph.D. Student, Department of Chemical and Biological Engineering, 2130 Biorenew Lab, 617 Bissell Rd.

ΔH_R	=	Heat of reaction, J mol^{-1}
ID	=	Inner diameter
ISRU	=	In-situ resource utilization
k	=	Thermal conductivity of fluid, W m^{-2} K^{-1}
k_{bed}	=	Stagnant bed thermal conductivity, W m^{-2} K^{-1}
k_{cat}	=	Thermal conductivity of catalyst, W m^{-2} K^{-1}
k_e	=	Equilibrium rate, as a function of temperature, $k_e(T) = \exp[(1.0/1.987)(56{,}000T^{-2} + 34{,}633T^{-1} - 16.4\ln(T) + 0.00557T) + 33.165]^1$, atm^{-2}
k_{eff}	=	Effective radial thermal conductivity, W m^{-2} K^{-1}
k_o	=	Rate constant, = 491,388.9^1, s^{-1} atm$^{-0.125}$
MW	=	Molecular weight of mixture, kg mol^{-1}
n	=	Experimental correction factor from Lunde[1], = 0.225
N	=	Molar flow rate, mol s^{-1}
Nu	=	Nusselt number, dimensionless
OD	=	outer diameter
p	=	Partial pressure, atm
P	=	Pressure, atm
Pe	=	Peclet number, (= $u_{avg}D_p\rho Cp/k$), dimensionless
Pr	=	Prandtl number, (= $Cp\,\mu/k$), dimensionless
r	=	Reaction rate of disappearance of CO_2, mol m^{-3} s^{-1}
r'	=	Radial coordinate
R	=	Ideal gas constant, J mol^{-1} K^{-1} or Pa m^3 mol^{-1} K^{-1}
Re	=	Reynolds number, (= $\rho V_{avg}D_h/\mu$ and $\rho V_{avg}D_p/(1-\epsilon)\mu$), dimensionless
Ru	=	Ruthenium
sccm	=	Standard cubic centimeters per minute
T	=	Temperature, K or °C
TC	=	Thermocouple
u_{avg}	=	Average velocity, m s^{-1}
U_{eff}	=	Effective overall heat transfer coefficient, W m^{-2} K^{-1}
v_i	=	Stoichiometric coefficient for species i, v_{H2}= -4, v_{CO2} = -1, v_{CH4} = +1, v_{H2O} = +2
V	=	Reactor volume variable, m^3
V_R	=	Total Reactor volume, m^3
X	=	Conversion
XPS	=	X-ray photoelectron spectroscopy
XRD	=	X-ray powder diffraction
y	=	mole fraction
Z_1	=	Inner reaction chamber radius, m
Z_2	=	Outer reaction chamber radius, m

Greek Letters:

β	=	Ratio of the surface area at heat transfer interface to reactor volume, m^{-1}
ε	=	Fixed-bed porosity or void fraction
λ	=	Wavenumber, nm
η	=	Effectiveness factor
ρ	=	Mass density, mol m^{-3}
μ	=	Dynamic viscosity, mol m^{-1} s^{-1}
ξ	=	Fluid-to-solid thermal conductivity ratio, dimensionless

Indices:

i	=	species
0	=	initial
f	=	feed into reactor

I. Introduction

THE success of sustainable human exploration and habitat development will rely on the explorers to survive from resources that are available from the explored planet or surrounding region. This concept of 'living off the land' is called In-Situ Resource Utilization (ISRU). On Mars, ISRU can include concepts such as capturing water that is trapped within regolith, utilizing radiation protection from lava-tubes, and using the sunlight to convert solar energy into electrical power.[2–4] In this paper, the particular concept of harvesting water and fuel from the Mars atmosphere via cryocoolers and the Sabatier reaction is discussed, with a specific investigation of the thermal and kinetic behavior of the
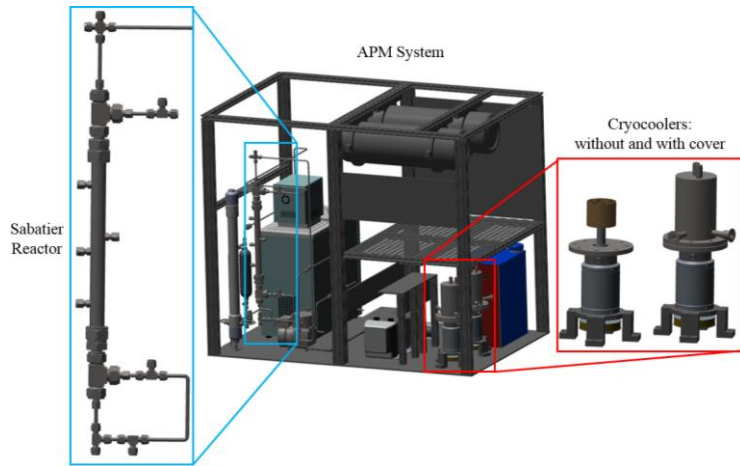
Figure 1. APM system model. Left: Sabatier reactor; Right: Cryocoolers.

Sabatier reactor. At Kennedy Space Center (KSC), the Atmospheric Processing Module (APM) first collects CO_2 from a simulated Martian atmosphere (95.4% CO_2, 3.0% N_2, and 1.6% Ar) and Martian pressure (~8-10 Torr) using dual cryocoolers.[5] The CO_2 is collected by flowing the Mars simulated atmospheric gas into the cryocooler chamber where a copper cold head is cooled to 150 K. The CO_2 that is isolated on the cryocooler cold head at 150 K as solid ice is then sublimated and stored at a higher pressure (6.8 atm) before it is introduced into the Sabatier subsystem (~ 2.72 atm). A 3-dimensional model of the main APM components was made with Parametric Technology Corporation Creo Elements software and is displayed in Figure 1. The Sabatier reactor is shown in the enlarged box to the left, and the cryocoolers are in the enlarged box to the right. The cryocooler is shown with and without its cover to display the high surface area copper cold head fitting. Details of the APM cryocooler and Sabatier subsystem are also discussed in detail elsewhere.[5,6] The Sabatier reaction, listed in Equation Eq. (1), is an exothermic reaction ($\Delta H = -165.4$ kJ/mol) where CO_2 is reduced by H_2 at elevated temperatures over a selective catalyst to produce CH_4 and H_2O.

$$CO_2 + 4H_2 \rightarrow CH_4 + 2H_2O \tag{1}$$

On APM, the H_2O vapor is condensed out of the product stream, collected in a vessel, and weighed. In the future, it will be sent to the Water Cleanup Module where it will be cleaned for preparation of water electrolysis, which will yield O_2 that can be stored and liquefied into cryogenic fuel as well as H_2 which can be recycled back to the Sabatier subsystem to produce CH_4. The CH_4 can be purified and stored before liquefaction for use as fuel, since the primary fuel for a Mars ascent vehicle is LO_2 and LCH_4.[7] The concept of the ISRU propellant production system to fuel a Mars ascent vehicle is also discussed in detail elsewhere.[4]

Sabatier reactors emit heat and are sensitive to many thermal and system conditions, so thermal control is imperative for catalytic efficiency and reaction success. On Mars, the low atmospheric pressure and large temperature swings reduce thermal conductance and cause temperature inconsistencies, and thermal controls will be required. Autonomous operation of a chemical system such as APM is needed to operate for approximately 500 days to generate the required fuel for a return vehicle. The fuel production for an ascent vehicle will require approximately 8-10 times more production than the current scale of the APM Sabatier reactor. It is necessary to determine the correct reactor volume that produces enough resources, while not overheating or generating unwanted byproducts. Modeling has begun to characterize the current Sabatier reactor and compare computational results with experimental data, in order to understand how to better design future versions of scaled up systems. Modeling the system will also aid in continuous control, as thermal runaway can cause catalyst and system hardware damage.

II. APM Sabatier Reactor Subsystem and Characterization

A. The APM Sabatier Subsystem

A simplified APM fluid schematic of the Sabatier subsystem is displayed in Figure 2. H_2 was first fed into the reactor at 1000 sccm during a preheat treatment from a room temperature k-bottle, until 210 ℃ was achieved inside of the catalyst bed. This H_2 reduction step was necessary for catalyst performance. At 210 ℃, H_2 flow was increased
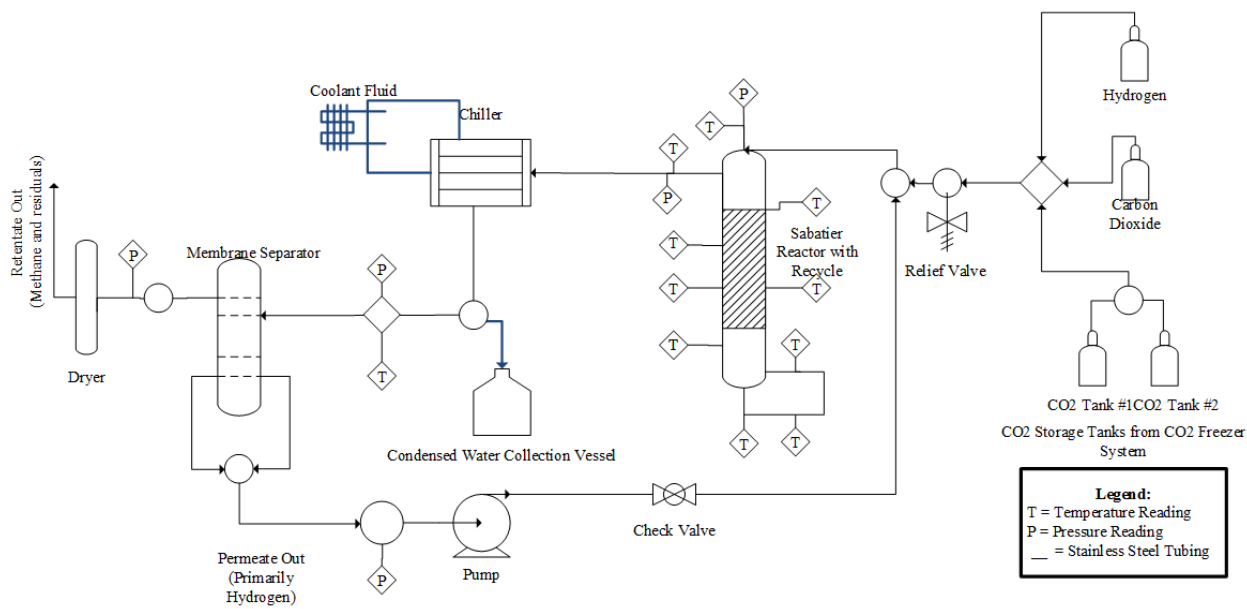
Figure 2. APM Sabatier subsystem schematic.

to 3375 sccm and CO_2 was introduced at 750 sccm, and the subsequent temperature rise indicated that the exothermic Sabatier reaction had begun. The flow, temperature, and pressure were observed and controlled with LabVIEW software. The initial feed ratio of H_2 to CO_2 was 4.5:1 to allow excess H_2 to recycle throughout the system. After the reaction was initiated and a catalyst temperature between 400 and 420 ˚C was achieved, the H_2:CO_2 molar ratio was reduced to 4:1. The CH_4 and H_2O vapor products were separated via a shell and tube heat exchanger (chiller/condenser system). Water production was measured by periodically removing water from the water collection vessel and measuring the mass. The CH_4 was separated from excess H_2 and unreacted CO_2 with a membrane separator. CH_4 purity was detected with a Varian Micro Gas Chromatograph (GC). The permeate stream containing H_2, unreacted CO_2 and a small amount of CH_4 was recycled back to the Sabatier reactor via a pump to complete the reaction. The membrane separator relied on a 1.92 atm pressure differential to produce >99.9% pure CH_4. The retentate side of the membrane was 2.38 to 2.72 atm and the permeate side was approximately 0.75 atm. This pressure differential was set manually with a back pressure regulator and required adjustment during any off nominal reading, but can be automated in the future. Unwanted byproducts of the reaction included carbon monoxide (CO), and could be detected by the GC. CO forms due to changes in feed ratio conditions or changes in temperature. With nominal temperature and pressure conditions, the reactor operated at steady state production with the H_2 recycle loop for 7 continuous hours.

Figure 3 shows a model of the Sabatier Reactor. The reactor is a stainless steel tube that is 30 cm long with an outer diameter (OD) of 2.54 cm and a wall thickness of 0.2 cm. The reactor is filled with 88 grams of 0.5 weight percent ruthenium supported on aluminum oxide (Ru/Al_2O_3) cylindrical catalyst pellets (3 mm) supplied by Sigma-Aldrich. Ru/Al_2O_3 catalyst is a proven catalyst with high CH_4 selectivity.[1,8] The reactant gas entered a feed pipe in the center of the reactor so that some of the excess heat of the reaction was used to preheat the incoming gas. The preheat loop was used as a heat sink to remove some of the heat from the reaction and avoid reactor thermal runaway. Four protrusions on the main portion of the reactor are fixtures for thermocouples (TC) to measure the temperature inside the catalyst bed (TC 6, 8, 9, 10). TC 5 is located on the OD of the reactor tube, and TC 14 was inserted inside the preheat tube at varying locations (A, B, C) to determine the preheat tube gas temperature. TC 14 was used only for preheat temperature measurements, and was removed during nominal operation. TC 15 and TC 7 measured the inlet and outlet of the preheat tube, respectively, and were also added only for experimental validation and removed during
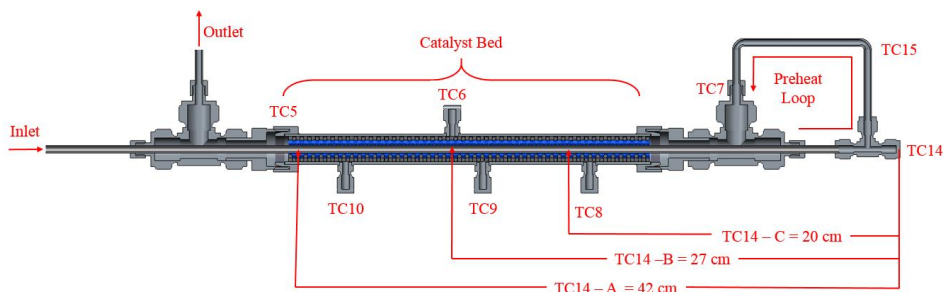

Figure 3. Cross-sectional view of Sabatier reactor model.

4

International Conference on Environmental Systems

nominal testing so as not to interfere with gas flow. The reactor was wrapped with a layer of heat tape (for preheating) and was covered with a layer of insulation to maintain as close to an adiabatic condition as possible.

B. APM Catalyst Characterization

In 2015, after several months of successful nominal testing, the reactant flow rates were purposely varied from nominal conditions in order to characterize reactor flow performance limits. CO, an unwanted byproduct, was detected by the GC in the product stream during a high flow rate experiment (1250 sccm CO_2 and 5000 sccm H_2). The maximum observed temperature was 586 ˚C which was well above the 400 ˚C nominal temperature value, but under the 600 ˚C safety shutdown temperature value. Although 600 ˚C was not observed by a thermocouple, thermal hotspots higher than 586 ˚C could have been present. The Sabatier reaction was unable to run at nominal
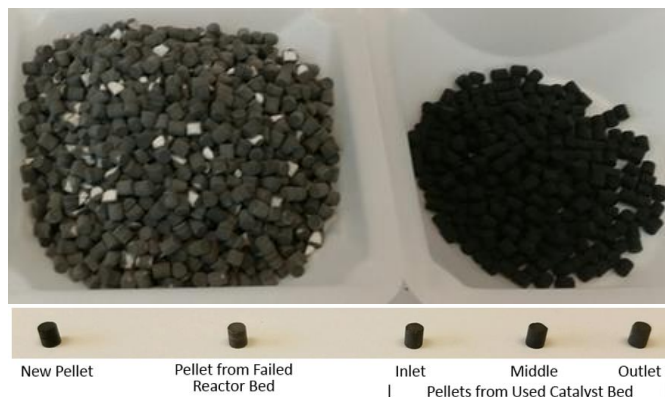

Figure 4. Top: Left: The 2015/spent catalyst that was damaged; Right: New/unused catalyst; Bottom: Ru/Al₂O₃ pellets that were characterized.

conditions after this run, so it was determined that the catalyst was damaged. The catalyst was removed (Figure 4) and some pellets were broken along with residual powders, and the catalyst had turned gray. The catalyst was replaced in the reactor bed with a fresh, unused batch of catalyst pellets and the reactions performed nominally once again.

A Sabatier catalyst failure study was initiated after this event, and led to the computational modeling development effort, with the aim of developing a model that could determine acceptable flow rates and predict temperature profiles in order to avoid damaging the catalyst and troubleshoot system tolerances. Five Ru/Al₂O₃ pellets were analyzed from the APM project during the catalyst investigation. They are shown in the bottom of Figure 4 and included a new pellet that was unused, a pellet from the Sabatier reactor that failed in 2015 after overheating and running the reactor at higher experimental flow rates, and samples from the current nominal Sabatier reactor in its three temperature zone regions: catalyst bed inlet, catalyst bed middle, and catalyst bed outlet.

X-ray powder diffraction (XRD) patterns were obtained from fresh and used catalysts in air at room temperature, using a PANalytical Empyrean machine with Cu Kα radiation (λ = 0.15406 nm) at a scan rate (2θ) of 0.02˚ s^{-1}. The accelerating voltage and applied current were 40 kilovolts and 40 milliamps, respectively. The samples were first prepared by grinding the pellets into powder form. Then, additional pellets from the used (but not damaged) catalyst bed inlet, middle, and outlet were prepared by scraping off the black/gray Ru layer and separating it from the white Al₂O₃ support. All the XRD prepared powders were ground in acetone with a silicon carbide mortar and pestle. The solids were extracted from the ground solution with a pipette and placed on the powder sample holder to accumulate in an even powder layer and dry in air before analysis. The International Centre for Diffraction Data library was used from the PANalytical XRD HighScore software for reference peak validation.

X-ray photoelectron spectrometry (XPS) measurements were conducted with a Thermo Scientific K-Alpha instrument using Al Kα radiation on the whole pellets (not the powders of Ru separated from the Al₂O₃ support). Surface survey scans and depth profiling were collected on the pellets. The depth profiling used a 3000 eV etch energy, 5 second etch cycle, at ~0.35 nm of etching per second. The reference C1s for this work was 284.91 eV.

III.   Small Scale Sabatier Reactor

Thermal and chemical computational modeling on the APM system with a preheat loop posed more challenges than the model of a simple packed bed reactor with no internal preheat tube. A small scale Sabatier reactor was set up and experiments were run to aid in model validation and compare with some of the literature results found on packed bed reactors. The reactor described earlier (Figure 5) used in APM experiments was denoted as "APM Sabatier reactor" in this work while the smaller reactor was denoted as "small scale Sabatier reactor". The model assumptions and equations were slightly different in each Sabatier reactor, and the differences will be discussed in the "Model Assumptions and Equations" section.

A. Small Scale Sabatier Reactor Description

The small scale Sabatier reactor consisted of a 304L stainless steel tube that was 1.25 cm OD and 1.1 cm ID. The reactor was packed with two different bed lengths of the same Ru/Al₂O₃ catalyst pellets as used in the APM Sabatier reactor. The bed lengths tested were approximately 4.5 cm and 8.89 cm long, yielding catalyst volumes of 2.3 ml (2.18

g) and 6.3 ml (6.67 g) respectively. The schematic of the reactor and different bed lengths is shown in Figure 5, with the catalyst bed located in the shaded/crosshatch area of the drawing. The 4.5 cm bed matched closely with the diameter of that found and modeled in literature[8], which provided additional literature for data validation. Five TCs, labeled A – E, were placed on the outside wall as shown in the figure. TC F was placed in the center of the catalyst bed and TC G was at the end of the catalyst bed. The reactor was sealed with Swagelok fittings and wrapped with heat tape (for pre-heat) and a layer of insulation.

The reactor was operated by pre-heating the catalyst bed until it reached ~250 °C under a H_2 flow. The gas flow is from left to right in the schematic. The CO_2 flow was started and once the reactor temperature increased, the heating tape was turned off. The H_2 to CO_2 ratio was 5:1 in all of the tests, and multiple flow rates were varied at each reactor volume, with the reactor pressure at 2.7 atm in all experiments. The reported reactor temperatures and CO_2 conversion percent were measured after the reactor temperatures had stabilized (approximately 1 to 3 hours of operation).
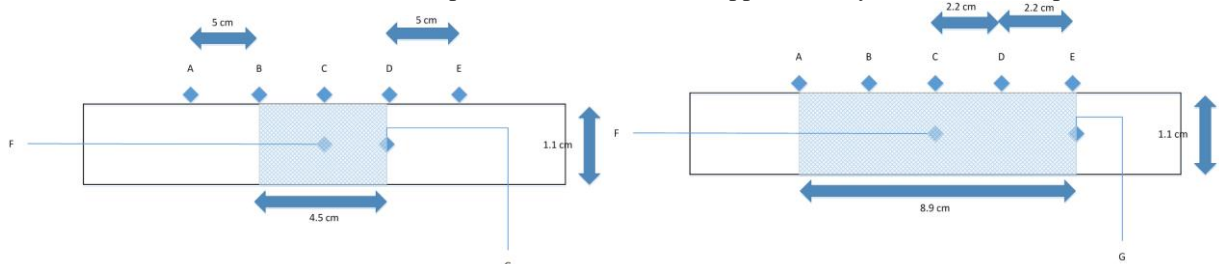

Figure 5. Left: 2.3 ml of catalyst; Right: 6.3 ml of catalyst.

IV. Model Assumptions and Equations

The initial section of the model description describes the assumptions and equations for the APM Sabatier reactor. The last section will describe the modifications made for the small scale Sabatier reactor. The Sabatier reactor model was first developed using Python software. The model aimed to characterize the Sabatier reactors in terms of tracking the temperature and the ratio of the various components in the mixture throughout the reactor (i.e. mole fraction, y_i). The first iteration of the model was simple, while future versions will add complexity in order to increase accuracy. The Python script worked by breaking the reactor domain into incremental pieces and solving equations within each segment. Figure 6 shows an example of a single segment along the reactor volume (ΔV). The current model maintained a stoichiometric ratio of 4:1 for the reactant gases H_2:CO_2 for validation, with the ability to modify this ratio in the future. The initial assumptions made on the system were as follows:

1. Plug flow conditions were in the reactor bed (no radial profile).
2. Axial diffusion in the reactor bed was neglected.
3. The system was at steady state.
4. The outer wall of the reactor was adiabatic.
5. No side reactions occurred.
6. Ideal gas laws applied.
7. Uniform porosity existed throughout the catalyst bed.
8. The effectiveness factor, η, was 1.

Figure 6. Reactor domain segment.

All known variables (flow rate, inlet temperature, initial species, etc.) were defined at the beginning of the program. The main function of the program is outlined in the flow diagram in Figure 7. This function determined the differential equations that define the change in species, reactor temperature, feed temperature, and pressure drop based on the inlet conditions for a given domain segment. The integration of these equations across the entire volume determined the conversion and temperature profile of the reactor.

The "Calculate Mass-Weighted Fluid Properties" function used a library of thermophysical properties that calculated fluid properties for the mixture of chemical species at the specified reaction temperature based off of the mass of each chemical species present. The fluid properties were taken from a NIST database.[9] The fluid properties included *Cp*, *ρ*, *k*, and *μ* as well as an updated average velocity of the fluid based on the density change. *Cp* was calculated using polynomial coefficients.[10] The specific heat polynomial coefficients for enthalpies of formation were gathered from literature.[11] The fluid properties were used to determine the effective overall heat transfer coefficient; this determined the amount of heat transferred between the reactor and feed which drove the change in temperature of each throughout the volume. A change in pressure was calculated based off of the updated fluid properties as well. The species composition changed based on the reaction rate for the given pressure and temperature conditions.
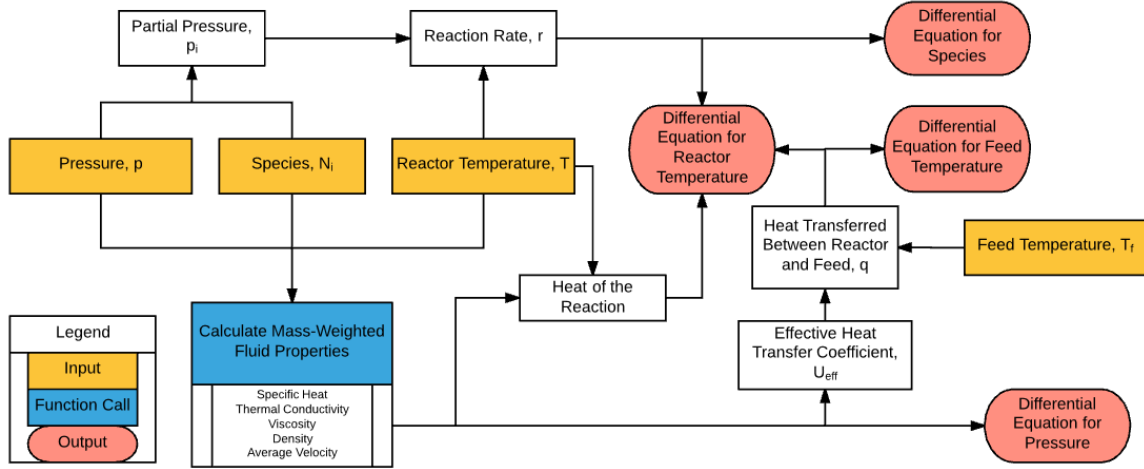
6

Figure 7. Main Python programming function flow diagram.

A. Kinetics

Some literature has modeled the rate of the overall Sabatier reaction via the Hougen-Watson rate equation [12] as well as empirically [1,8]. The empirically derived method was used in this work which modeled the rate of disappearance of CO_2 and is shown in Eq. (2).

$$r = k_0 \exp(-E_a/RT)\left\{[p_{CO_2}]^n [p_{H_2}]^{4n} - \frac{[p_{CH_4}]^n [p_{H_2O}]^{2n}}{[K_e(T)]^n}\right\} / (RT) \tag{2}$$

B. Material Balance

The steady state mass balance of the reactor [14] was calculated using Eq. (3), and conversion of CO_2, X, was calculated using Eq. (4). The internal effectiveness factor is a measurement of how far the reactants diffuse into the pellet before reacting. In essence, it measures how effectively the catalyst is being used. When it is less than 1, it is diffusion limited, and when it is near 1, the pellet is reaction limited.[13] In this work, it was assumed that $\eta = 1$. The intrinsic kinetics on the surface of the catalyst pellet have not been studied in great detail for non-isothermal reactions. We hope to study the non-isothermal conditions and effect of diffusion limitations by the catalyst in future work.

$$\frac{dN_i}{dV} = v_i \eta r \tag{3}$$

$$X = 1 - \frac{N_{CO2}}{N_{CO2,0}} \tag{4}$$

C. Pressure Drop

For slim packed tubes, wall effects are an important factor when considering the pressure drop across the packed bed. An appropriate correlation for a packed bed with cylinders was given by Reichelt.[15] The pressure drop equation is given in Eq. (5).

$$\frac{dP}{dV} = -\frac{MW}{Ac}\left[\frac{190 A_w^2 u_{avg} \mu}{D_p^2}\frac{(1-\varepsilon)^2}{\varepsilon^3} + \frac{A_w u_{avg} \rho}{B_w D_p}\frac{(1-\varepsilon)}{\varepsilon^3}\right]/101325 \tag{5}$$

where,

$$A_w = 1 + \frac{2}{3(D_h/D_p)(1-\varepsilon)} \qquad\qquad B_w = \left[2.00\left(\frac{D_p}{D_h}\right)^2 + 0.77\right]^2$$

D. Energy Balance

The amount of heat transferred between the reactor and feed gases determined the temperature profile through the reactor domain. The methodology by which it was calculated was the thermal resistance method. An overall heat transfer coefficient was calculated based on the average effective radial thermal conductivity of the bed and the convective heat transfer along the wall, resulting in Eq. (6)[16].

$$\frac{1}{U_{eff}} = \frac{1}{h} + \frac{1}{6}\left(\frac{Bi + 3}{Bi + 4}\right)\frac{D_h}{k_{eff}} \tag{6}$$

The convective heat transfer coefficient is calculated by the Nusselt number correlation as suggested by Martin & Nilles[17] shown in Eq (7).

$$Nu = \frac{h\,D_h}{k} = \left(1.3 + 5\frac{D_p}{D_h}\right)\left(\frac{k_{eff}}{k}\right) + 0.19Re^{0.75}Pr^{0.33} \tag{7}$$

The effective radial thermal conductivity is given by Eq. (8) based on correlations by Winterberg.[18,19] The radial average of Eq. (9) was used in the calculation of Eq. (8).

$$k_{eff} = k_{bed} + \frac{1}{8}Pe\,f(Z_2 - r')\,k \tag{8}$$

$$f(Z_2 - r') = \begin{cases} \left(\dfrac{Z_2 - r'}{\left(0.44 + 4exp\left(-Re/70\right)\right)}\right)^2, & Z_1 < Z_2 - r' \le D_p\left[0.44 + 4exp\left(-Re/70\right)\right] \\ 1, & Otherwise \end{cases} \tag{9}$$

The stagnant bed conductivity based on work by Zehner and Schlunder[20,21] was calculated from Eq. (10).

$$\frac{k_{bed}}{k} = 1 - \sqrt{1 - \varepsilon} + \frac{2\sqrt{1-\varepsilon}}{1-\xi B}\left[\frac{(1-\xi)B}{(1-\xi B)^2}ln\left(\frac{1}{\xi B}\right) - \frac{1}{2}(B+1) - \frac{B-1}{1-\xi B}\right] \tag{10}$$

Where $\quad \xi = \dfrac{k}{k_{cat}} \quad$ and $\quad B = 2.5\left(\dfrac{1-\varepsilon}{\varepsilon}\right)^{10/9}$

The constant calculated from Eq. (11) was used to calculate the heat transfer along the interface between the reactor and internal feed pipe. It is a ratio of the surface area of the feed pipe to the reactor cross-sectional area.

$$\beta = \frac{4\,ID}{OD^2 - ID^2} = 62.19 \tag{11}$$

The energy balance for the reactor for a single reaction and only one heat transfer boundary, is shown in Eq. (12). When integrated across the volume, this equation determined the temperature of the reactor.

$$\frac{dT}{dV} = \frac{-\Delta H_R r + U_{eff}\beta(T_f - T)}{\sum_i N_i Cp_i} \tag{12}$$

Because there was no reaction within the internal feed tube, the energy balance in the feed tube only included heat transferred between the reactor and feed gas, as described by Eq. (13).

$$\frac{dT_f}{dV} = \frac{U_{eff}\beta(T_f - T)}{\sum_i N_{i,f} Cp_{i,f}} \qquad Where, \quad T_f|_{V=V_R} = T_{f0} \tag{13}$$

In order to find steady state conditions, a "shooting strategy" was used. An initial guess for the reactor inlet temperature was provided to the model, and integration over the reactor volume yielded an inlet feed temperature value for the specified reactor inlet temperature. This value was compared to the known inlet feed temperature and iterated until there was a match. A sample output from this iteration of reactor conditions is shown in Figure 8. The intersection points indicated a steady-state condition. There is a caveat to the boundary condition at the reactor inlet/feed outlet. Based on experimental results, there is some heat leak through the preheat loop as a result of imperfect insulation. While the amount of this heat leak is difficult to quantify, the model attempts to incorporate this based on a specified temperature difference (T_{diff}) between the feed outlet and the reactor inlet.

E. Small Scale Sabatier Reactor Equations

The same kinetic and material balance equations (Eq. (2) through (4)) were utilized for the small scale Sabatier reactor along with the same pressure drop equation (Eq. (5)). While a major difference between the two reactors was the lack of external cooling and internal feed tube, the same energy balance equation (Eq. (11)) was also used. The results section will discuss why this term was included in the energy balance. The model can predict the results of adiabatic operation by setting the effective heat transfer coefficient to zero.
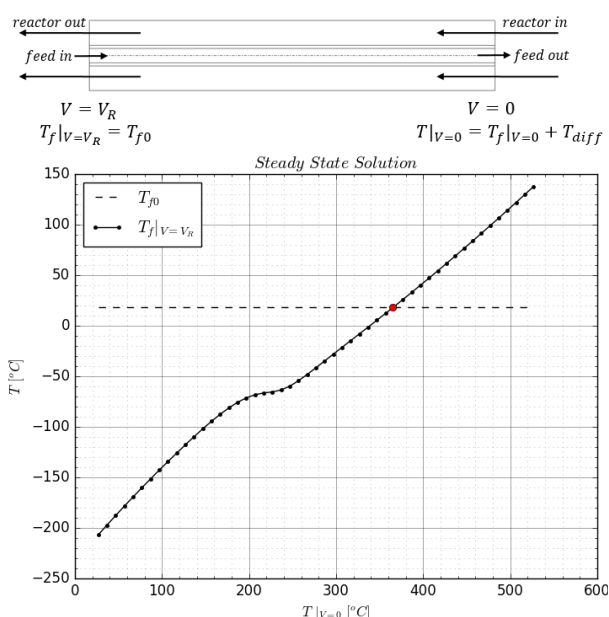

Figure 8. Top: Reactor domain boundary conditions; Bottom: Steady-state determination for inlet reactor temperature.

V.   Results and Discussion

A. APM Sabatier Reactor Experimental and Modeling Results

Long duration (7 hour) runs were performed on the reactor to determine steady state reaction temperatures during nominal operation of CH_4 production. The results of the thermocouple temperatures at steady state for nominal conditions (with H_2 recycle loop on) and for single pass conversion (no H_2 recycle loop) are displayed in

Table 1 and Figure 9. At nominal conditions and steady state, >99% conversion of CO_2 to CH_4 was performed and validated via GC, along with 32 grams per hour of H_2O production. TC14-C was the highest temperature of the preheat tube, at 327 °C for nominal conditions, and TC 8, near the reactor inlet, was the hottest spot of the entire system. Due to thermocouple spacing, it was possible that there were regions at higher or lower temperature than recorded by TC locations. The catalyst bed reactor inlet, and catalyst bed reactor outlet were 260 °C different in temperature during for nominal conditions. By the time the gases left the reactor outlet, they were cooled down to the point where the Sabatier reaction was not expected to have much activity and were also interfacing with the coolest part of the preheat tube (87 °C at TC 14-A), which also decreased the temperature. The reaction should have the highest conversion near the catalyst bed inlet and then subside as it travels out of the reactor bed and leaves the system. Because of the lower temperature profile (<300 °C), the reactor may be oversized for nominal flow rate conditions, but there is a threshold of higher throughput flow rates, as observed with catalyst damage occurring at 1250 sccm CO_2 and 5000 sccm H_2.

Table 1. Temperature averages at steady state for a nominal run, displayed in °C

H_2/CO_2 flow rate, sccm	Recycle loop on? Y/N	TC14-A (Preheat 42 cm)	TC14-B (Preheat 27 cm)	TC14-C (Preheat 20 cm)	TC15 (loop inlet)	TC7 (loop exit)	TC8 (inlet)	TC6 (mid.)	TC9 (mid.)	TC10 (out)	Single Pass CO_2 conversion, %
750/3000	Y	87	192	327	142	132	425	264	254	165	-
250/1000	N	-	-	431	59	54	448	183	174	129	95
350/1400	N	-	-	469	71	57	502	205	186	117	92
450/1800	N	-	-	505	93	70	541	252	227	121	92
550/2200	N	-	-	527	113	82	564	297	270	129	91
650/2600	N	-	-	539	132	95	575	335	307	135	88

9

For single pass conversion, the flow rate was gradually increased from a H_2/CO_2 flow rate of 750/3000 sccm to 650/2600 sccm. As the flow rate was increased, the conversion of CO_2 in the system declined. The addition of the recycle stream allows more complete conversion of the

Figure 9. Temperature profile through APM Sabatier reactor at steady state conditions.

CO_2. This could be due to the fact that a small additional stoichiometric amount of H_2 is available, and also additional gas from the cool recycle stream helps control thermal stability in the catalyst bed.

The results of the single pass Python model for temperature profiles across the normalized reactor volume are shown in the left of Figure 10. The input CO_2/H_2 flow rates of 650/2600 sccm were used for these images. The feed tube temperature inside the reactor was manually input from experimental data. The experimental results of the catalyst bed thermal profile (blue dashed line), labeled T, and were much lower at the inlet than the model predictions (blue solid line). At >600 ˚C, the catalyst would become damaged and the reaction would shift its hot spot location towards the middle and outlet regions of the reactor catalyst bed to achieve conversion. The model predicted a decrease in temperature across the volume of the reactor, which was observed experimentally as well. T_f was the reactor feed temperature, which at this case experimental values were inserted into the model. Some adjustment is needed in the thermal prediction of the model for the preheat loop and inlet conditions, as the area of heat loss in this region is not entirely accounted for in the code. It is expected that as pellet considerations are also modeled, the predictions will become more accurate.

The conversion calculated from the Python model is displayed in the right of Figure 10. Approximately 80% conversion is achieved by the time the reactor is 40% along the volume of the reactor. This result matched well with the thermal profile

Figure 10. Python model results for the APM Sabatier reactor. Left: Temperature profile across the normalized volume of the reactor; Right: Conversion across the normalized volume of the reactor.

as it decreased in temperature, and so most or all of the conversion would have already been achieved in the expected 400 ˚C temperature range at the reactor inlet region. The trends match empirical data for a 4:1 $H_2:CO_2$ fed reaction and follow what would be expected of a single pass conversion of 88%.

The Python model results of the reactants and products displayed as mole fractions during nominal conditions of the APM Sabatier reactor across the normalized volume is show in Figure 11. The trends also match empirical data for a 4:1 $H_2:CO_2$ fed reaction and follow what would be expected of the single pass conversion of 88%.

In general the Python model results and trends were quite accurate to the experimental results. Future additions to the model will include more experimental conditions, such as the heat loss to the environment (the lab system was not a truly adiabatic system), H_2 recycle stream, and nonisothermal considerations on the
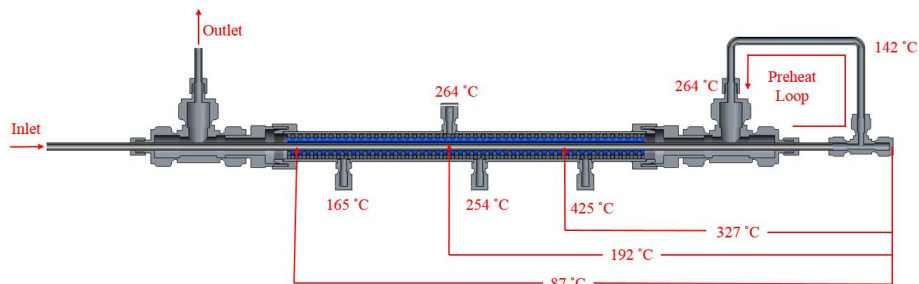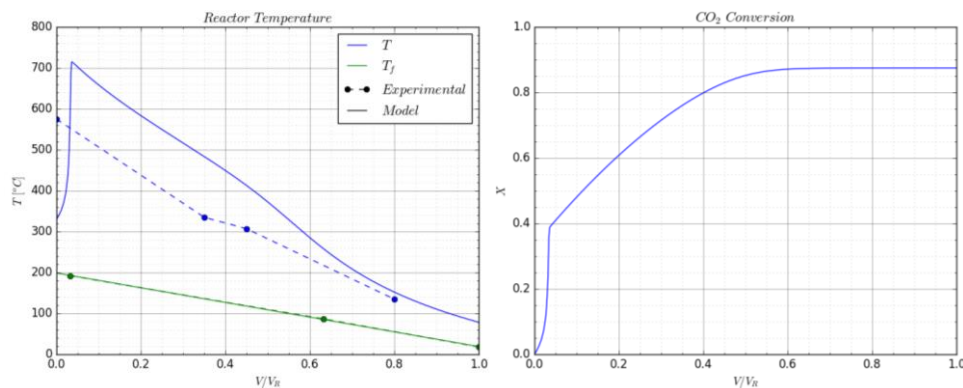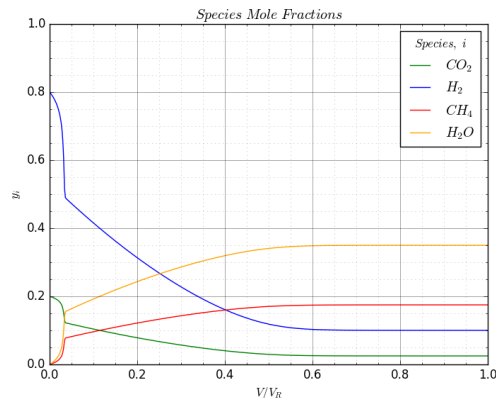

Figure 11. Mole fraction of reactants and products during nominal conditions of the APM Sabatier

10

catalyst surface. Current equipment is limited in how many TCs can be added, and thermal hot spots may be undetected at this time. The model will help determine these expected hot spot regions, and TCs can be placed appropriately.

B. Small Scale Sabatier Reactor Experimental and Modeling Results

The experimental results of the small scale single pass Sabatier reactor temperature profile is shown in Table 2. 98% conversion was achieved at the lowest flow rate of the 2.3 ml catalyst bed volume, which had the highest temperature of 376 ˚C at the middle of the catalyst bed, while maintaining the lowest maximum temperature of all 2.3 ml runs. Total flow rates less than 240 sccm were not evaluated, because at this low flow, the GC did not sample properly. As flow rate increased, the temperature in the catalyst bed increased, but conversion decreased. For the 6.3 ml catalyst bed, the same trend of decreased conversion at increased flow rate was observed. Since increasing the volume of the catalyst bed in this reactor resulted in a longer bed of the same diameter, the lowest flow rate evaluated was selected such that it was slightly lower than the maximum flow rate in the smaller volume reactor. Since 376 ˚C is roughly the high temperature needed for >98% conversion to CH_4, we can discuss possible scenarios for Mars Sabatier reactor development. If several small reactors can be placed in series and run at lower flows, the thermal integrity of the catalyst is protected, and >98% conversion is ideal. If one or two reactors are needed at high throughput of gas, the system may perform at lower conversion of CO_2, and also run the risk of thermal damage to the catalyst pellets (>600 ˚C).

Table 2. Experimental data from small scale Sabatier reactor.

Catalyst bed volume	CO_2/H_2 flow rate	Thermocouple, ˚C							Conversion
ml	sccm	A (surface inlet)	B	C (surface middle)	D	E (surface outlet)	F (catalyst bed middle)	G (catalyst bed outlet)	X
2.3	40/200	225	295	314	295	258	376	293	98
2.3	80/400	106	236	289	259	175	417	259	96
2.3	120/600	93	282	366	333	219	523	337	97
2.3	160/800	85	298	416	395	267	570	407	93
6.3	150/750	347	391	362	295	249	399	252	98
6.3	165/825	350	408	383	314	264	424	271	99
6.3	225/1125	364	455	454	398	345	501	355	97
6.3	275/1375	361	472	484	440	390	531	405	91
6.3	300/1500	355	478	494	456	410	542	427	85
6.3	350/1750	336	486	511	481	437	558	460	91
6.3	375/1825	329	485	516	489	449	564	471	82
6.3	425/2125	253	467	530	512	475	579	500	80

The Python model results of the small scale single pass Sabatier reactor is shown in Figure 12 and Figure 13.The images represent the larger bed volume (6.3 ml) and a CO_2/H_2 flow rate of 425/2125 sccm. If the operation is assumed adiabatic, the results indicate a very poor performance of the reactor as shown by the temperature and conversion profiles in the left side of Figure 12. By implementing the wall temperature profile as obtained from the experiment, a much more accurate set of results are predicted by the model as can be seen in the plots to the right in Figure 10 and Figure 13. With the adiabatic case, the entire reaction stops when it reaches the maximum temperature. It is apparent that some cooling is necessary to maximize the conversion within the reactor and that the experimental reactor is not as well insulated as assumed. The model predicts the hot spot is located approximately 25% into the reactor. In addition, the model for the non-adiabatic case shows that highest temperature in the bed exceeds 650 °C, which is thought to be high enough to damage the catalyst. This shows how the model can be used to determine that a particular reaction condition is not appropriate for the reactor.

The catalyst is above 600 °C for only about 1 cm of the reactor length. There can be only a finite number of thermocouples in the catalyst bed, and it is possible that the hot spot would be missed as occurred in this case.

C. APM Sabatier Reactor Catalyst Characterization Results

1. XRD Results

The XRD scan of the entire Ru/Al_2O_3 pellet from an unused pellet, a damaged pellet from 2015, and the current 2017 Sabatier reactor with a pellet from the reactor inlet, middle and outlet pellets is shown in Figure 14. The low intensity and broad peaks reveal that the material is amorphous. Since the diffraction peaks remain unchanged after
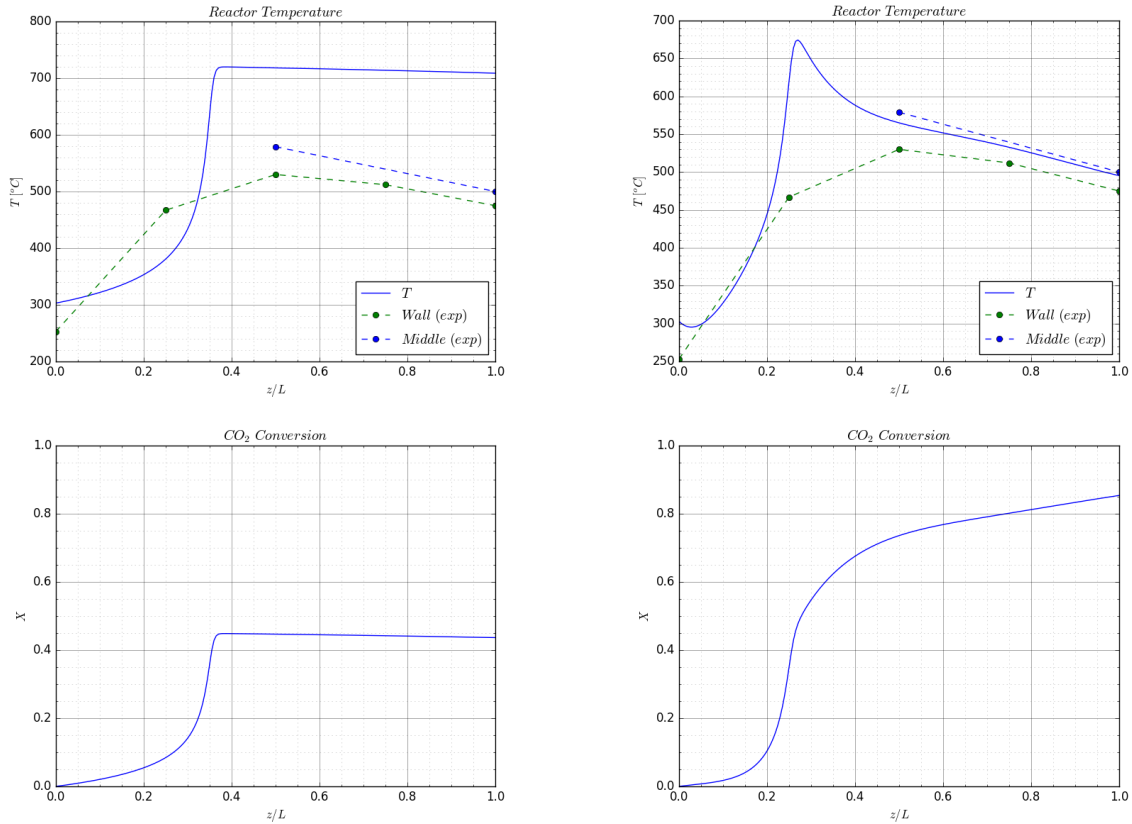
Figure 12. Python model results for the small scale Sabatier reactor. Left: Adiabatic operating condition; Right: Imposed wall temperature profile based on experiment.
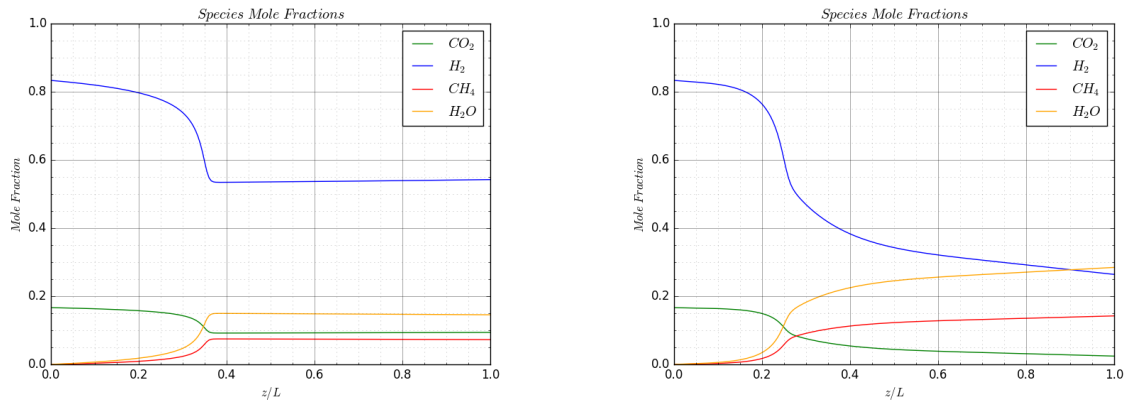

Figure 13. Species mole fraction profiles for the small scale Sabatier reactor. Left: Adiabatic operating condition; Right: Imposed wall temperature profile based on experiment.

and during use at elevated temperatures, no significant change in the crystallinity occurred pre- or post-reaction. The pellets show reflections corresponding to Al_2O_3 (▲) and RuO_2 (●). α-Al_2O_3 and γ-Al_2O_3 are the most common phases of Al_2O_3. α-Al_2O_3 is polycrystalline and typically used in ceramic applications, is the most stable, and calcined at high temperatures (>1000 ˚C), whereas γ-Al_2O_3 has high surface area, processed at lower calcination temperatures (~500 ˚C), and is typically used in catalyst applications. It is often observed in literature that that the γ-Al_2O_3 transforms into the α-Al_2O_3 phase at elevated temperatures.[22] It was confirmed by the catalyst vendor that the Sabatier pellets purchased for this were supported on γ-Al_2O_3.
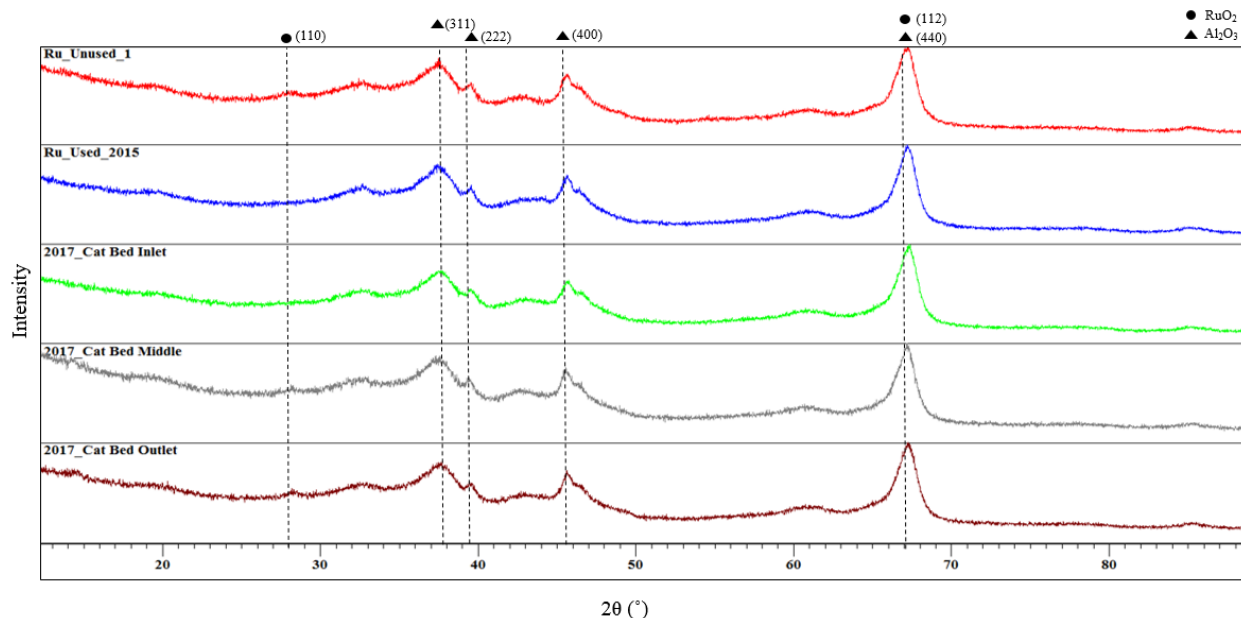
International Conference on Environmental Systems

Figure 14. XRD Spectrums of Ru/Al$_2$O$_3$ pellets from APM project, unused, used in 2015 (damaged), and used 2017 (not damaged).

The Al$_2$O$_3$ phases were observed at 37.8°, 39.5°, 45.5°, and 67° 2θ. The 37.8° and 67° 2θ were stronger in α-Al$_2$O$_3$, corresponding to the 110 and 214 reflections, respectively. Although faint, the value at 28.4° was most prevalent in the unused, catalyst bed middle, and catalyst bed outlet pellets, which corresponded to the RuO$_2$ 110 reflections. The unused catalyst has not been heat treated yet, and the catalyst bed outlet sustained the lowest temperatures during operation, so it was not participating in the high exothermic reaction conditions and likely not undergoing thermal shock like the inlet and middle catalyst bed were. At 39.5° and 67°, the 2θ values were also characteristic of the RuO2 200 and 301 reflections, respectively, but also overlap with the Al$_2$O$_3$ reflections at these locations. RuO$_2$ species was likely dispersed well on the Al$_2$O$_3$ support surface prior to high temperature (>200 ˚C) exposure. Confirmation of metal sintering or particle aggregation was challenging to determine via XRD since the pellets were ground in the aqueous phase during preparation for analysis. Even if sintering did occur at high temperature reaction conditions, the size of crystallite may not have grown large enough for XRD detection.[23]

The XRD scan of the Ru pellet powder and Al$_2$O$_3$ pellet powders from the current 2017 in-use Sabatier reactor system (used but not damaged) is shown in Figure 15, along with reference spectrums of the γ and α Al$_2$O$_3$ phases, Ru, and RuO$_2$. The main difference observed from these scans was the fact that the cooler portions of the catalyst bed (the outlet and middle) had reflections corresponding to RuO$_2$, while the hotter reactor inlet did not.

It was challenging to completely separate the powdered Ru coating from the Al$_2$O$_3$, and therefore some overlap was present when attempting to isolate the two materials. The reference reflections also overlap with the experimental reflections for the Ru, RuO$_2$, and Al$_2$O$_3$ patterns, especially for broad peak results. The reference α-Al$_2$O$_3$ matched closest with the support structure, but some of the reference γ-Al$_2$O$_3$ peaks were also present.

2. XPS Results

The XPS Ru3D scan for the Ru/Al$_2$O$_3$ pellet of an unused pellet, damaged pellet from 2015, and inlet, middle and outlet pellet of the current 2017 APM reactor (used but not damaged) are shown overlayed in the top of Figure 16. The left image (top of Figure 16) was at the surface (etch level = 0) and the right was at approximately 15.75 nm below the first oxide layer (etch level = 9). The chemical states of the Ru3d$_{5/2}$ spin orbit is 280.2 eV for Ru Metal and 280.7 for RuO$_2$.[24] On the surface (etch level = 0), the inlet, middle, and outlet of the 2017 APM reactor pellets were similar with binding energies of the right at ~280.2 and the left at ~284.6 eV. The unused pellet had the farthest shift to the left, and the used/damaged pellet had the farthest shift to the right. The same behavior was observed after etching away some of the surface oxide (etch level = 9), but the used pellet had similar binding energy to the 2017 pellets. Since γ-Al$_2$O$_3$ has higher surface area, the pores in the catalyst support may have collapsed during the phase change to α, encapsulating the Ru, which could be why it was not present in the hotter regions of the reactor, and the overall surface area of RuO$_2$ would decrease. This damage may have contributed to the catalyst inability to become successfully reduced for CH$_4$ selectivity.[24]

13

The XPS Al2p scan for the Ru/Al$_2$O$_3$ pellets are shown overlayed in the bottom of Figure 16 at the surface (left, etch level = 0) and at approximately 15.75 nm below oxide layers (right, etch level = 9). The primary XPS region of Al2p had binding energies for Al metal at 72.6 eV and Al oxide at 74.6 eV.[24] The damaged catalyst of 2015 had the farthest shift to the right, which could imply that Ru had been removed from the surface layers, leaving Al$_2$O$_3$ exposed. Unfortunately sputtering with Ar ions for etching can adsorb oxygen and reform oxide sites. The etch level 9 may show a healthy under layer of Al$_2$O$_3$ for all pellets with little shift or deviation. This could be the results of the damaged catalyst returning oxide layers due to the reactive surface of etching.

VI.   Future Work

Computational Fluid Dynamics (CFD) simulations are currently being conducted using STAR-CCM+ as a separate way to verify modeling results. The CFD approach allows the ability to incorporate 3D flow effects into the model. Because the ratio between the tube diameter to pellet size is low, it is important to include the non-uniformity of the flow and the wall bypassing effects that it may cause. The validity of certain simplifying assumptions in the Python model can be determined by comparing the results of the CFD to the Python script. Once the Python script is at an acceptable accuracy, it can be used to determine other suitable reactor geometry fairly quickly when compared to the more computationally expansive CFD approach. Figure 17 shows a close-up of the reactor domain mesh with the fluid in blue and the solid catalyst pellets in black.

There are also plans to expand the capability of the Python model to take into consideration the energy and mass balance across the catalyst pellets and effects of non-isothermal particle considerations. Since the reaction is exothermic, the catalyst pellet internal temperature may rise. We must keep track of two phases being affected by this reaction: the fluid-phase and the diffusion process on the solid-phase catalyst pellets. These phases are simultaneously exchanging mass and energy and will be modeled for their relationship to one another. The energy balance equations will be coupled into the enthalpy change on the fluid, and the enthalpy change on the particle. The Weisz-Prater criterion can be used to measure the rate of reaction to determine if there are any internal diffusion limitations of the reaction. The Mears' Criterion can be used to observe if external diffusion is limiting.[13]
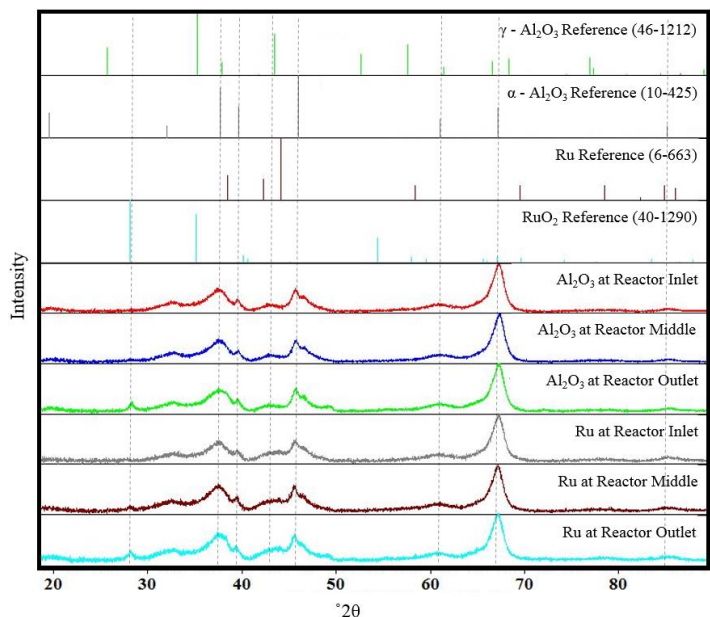

Figure 15. XRD Spectrums of Ru and Al$_2$O$_3$ isolated powders from the pellets from current APM Sabatier reactor.
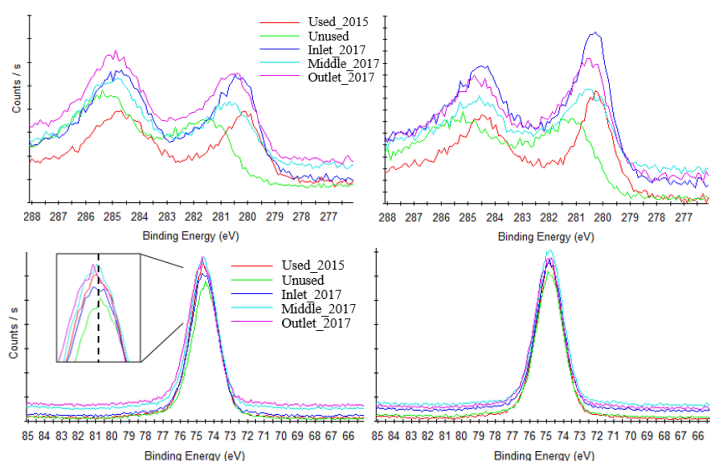

Figure 16. Top: Ru3d Overlay. Left: Etch Level 0, Right: Etch Level 9; Bottom: Al2p overlay. Left: Etch level 0, Right: Etch Level 9.
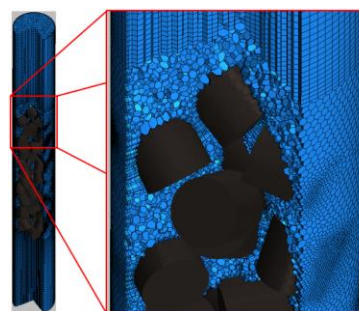

Figure 17. CFD reactor domain mesh with fluid (blue) and solid catalyst (black).

International Conference on Environmental Systems

VII. Conclusion

A thermal and kinetic model of the APM Sabatier reactor and small scale Sabatier reactor was created using Python. The model was developed after a catalyst performance failure occurred in the APM Sabatier reactor in 2015 during higher than nominal flow rate testing. Since high flow rates will damage the catalyst, the model will help optimize the throughput of the catalyst bed, and be validated experimentally to build trust in the model. The model will continue to evolve including considering transport by convection in the fluid, diffusion inside the catalyst pellets, reaction kinetics, and thermal effects of the gas-phase and solid-phase aspects of the reactor system. The reaction diffusion investigation of the catalyst will be coupled to the mass and energy balances of the fluid, as well as the pressure drop considerations across the reactor. The continued development of this modeling will allow us to optimize systems that can predict and determine acceptable flow rates and temperature profiles in order to avoiding damaging the catalyst and troubleshoot system tolerances. It will also help with scaling larger systems or systems in series for future design of a Mars ISRU propellant production system.

Ru/Al_2O_3 catalyst characterization analysis resulted in subtle changes that were observed in both XRD and XPS. The XRD crystal structure on the pellets that encountered higher reaction temperature (>500 ˚C) were missing RuO_2 characteristic reflections, and the cooler portions of the catalyst bed (reactor middle and outlet) had reflections corresponding to RuO_2, while the reactor inlet did not. The XPS observations revealed that a stronger oxide layer was present on 'healthy' or unused catalyst as well, but not present on the damaged catalyst. If the phase change from γ-Al_2O_3 to α caused pores to collapse and obstruct the surface layer of Ru, this may have been why performance for Sabatier selectivity and reaction temperatures declined. Overall, catalyst exposure to reaction temperatures greater than 450 ˚C caused the thermal shock on the catalyst surface, losing the ability to selectively form CH_4.

References

[1] Lunde, P. J., and Kester, F. L., "Rates of methane formation from carbon dioxide and hydrogen over a ruthenium catalyst," *Journal of catalysis*, vol. 30, 1973, pp. 423–429.

[2] Barker, D., Chamitoff, G., and James, G., "Resource utilization and site selection for a self-sufficient martian outpost," 1998.

[3] Arney, D. C., Jones, C. A., Klovstad, J., Komar, D. R., Earle, K., Moses, R., Bushnell, D., and Shyface, H., "Sustaining Human Presence on Mars Using ISRU and a Reusable Lander," *AIAA SPACE 2015 Conference and Exposition*, 2015, p. 4479.

[4] Kleinhenz, J. E., and Paz, A., "An ISRU propellant production system for a fully fueled Mars Ascent Vehicle," *10th Symposium on Space Resource Utilization*, 2017, p. 423.

[5] Muscatello, A. C., Hintze, P. E., Meier, A. J., Bayliss, J. A., Karr, L. J., Paley, M. S., Marone, M. J., Gibson, T. L., Surma, J. M., Mansell, J. M., Lunn, G. M., Devor, R. W., Captain, J. G., and Berggren, M., "Mars Atmospheric In-Situ Resource Utilization Projects At the Kennedy Space Center," American Society of Civil Engineering Earth and Space 2016 Conference, 2016.

[6] Muscatello, A., Devor, R., and Captain, J., "Atmospheric Processing Module for Mars Propellant Production," *Earth and Space 2014*, 2014, pp. 1–46.

[7] Mars Architecture Steering Group, NASA Headquarters, "Human Exploration of Mars Design Reference Architecture 5.0 Addendum," 2009.

[8] Lunde, P. J., and Kester, F. L., "Carbon Dioxide Methanation on a Ruthenium Catalyst," *Industrial & Engineering Chemistry Process Design and Development*, vol. 13, Jan. 1974, pp. 27–33.

[9] "Thermophysical Properties of Fluid Systems" Available: http://webbook.nist.gov/chemistry/fluid/.

[10] Cengel, Y., and Boles, M., *Thermodynamics: An Engineering Approach*, New York: McGraw-Hill Education, 2014.

[11] Kays, W. M., Crawford, M. E., and Weigand, B., *Convective Heat and Mass Transfer*, Boston: Mcgraw-Hill, 2004.

[12] Quatch, T. Q., and Rouleau, D., "Kinetics of the reaction between carbon dioxide and hydrogen over a ruthenium catalyst in a continuous stirred tank reactor," *Journal of Applied Chemistry and Biotechnology*, vol. 26, 1976, pp. 527–535.

[13] Fogler, H. S., *Elements of Chemical Reaction Engineering*, Upper Saddle River, NJ: Prentice Hall, 2005.

[14] Rawlings, J. B., and Ekerdt, J. G., *Chemical Reactor Analysis and Design Fundamentals*, Madison, Wis: Nob Hill Publishing, 2002.

[15] Reichelt, W., "Zur Berechnung des Druckverlustes einphasig durchströmter Kugel-und Zylinderschüttungen," *Chemie Ingenieur Technik*, vol. 44, 1972, pp. 1068–1071.

[16] Kiewidt, L., and Thöming, J., "Predicting optimal temperature profiles in single-stage fixed-bed reactors for CO2-methanation," *Chemical Engineering Science*, vol. 132, Aug. 2015, pp. 59–71.

[17] Martin, H., and Nilles, M., "Radiale Wärmeleitung in durchströmten Schüttungsrohren," *Chemie Ingenieur Technik*, vol. 65, Dec. 1993, pp. 1468–1477.

[18] Winterberg, A., Tsotsas, E., Krischke, A., and Vortmeyer, D., "A Simple and Coherent Set of Coefficients for Modelling of Heat and Mass Transport with and without Chemical Reaction in Tubes Filled with Spheres," *Chemical Engineering Science*, vol. 55, 1999, pp. 967–979.

[19] Dixon, A. G., "Fixed bed catalytic reactor modelling-the radial heat transfer problem," *The Canadian Journal of Chemical Engineering*, vol. 90, Jun. 2012, pp. 507–527.

[20] Zehner, P., and Schlünder, E. U., "Wärmeleitfähigkeit von Schüttungen bei mä\s sigen Temperaturen," *Chemie Ingenieur Technik*, vol. 42, 1970, pp. 933–941.

[21] Kandula, M., "On the Effective Thermal Conductivity of Porous Packed Beds with Uniform Spherical Particles," *Journal of Porous Media*, vol. 14, 2011.

[22] Sathyaseelan, B., Baskaran, I., and Sivakumar, K., "Phase Transition Behavior of Nanocrystalline Al2O3 Powders," *Soft Nanoscience Letters*, vol. 3, 2013, pp. 69–74.

[23] Chen, L., Zhu, Y., Zheng, H., Zhang, C., and Li, Y., "Catalytic degradation of aqueous Fischer–Tropsch effluents to fuel gas over oxide-supported Ru catalysts and hydrothermal stability of catalysts," *Journal of Chemical Technology & Biotechnology*, vol. 87, Aug. 2012, pp. 1089–1097.

[24] "Thermo Scientific XPS: Knowledge Base" Available: http://xpssimplified.com/periodictable.php.

International Conference on Environmental Systems